Two Recent Examples of X-Ray Magnetic Scattering Studies

Doon Gibbs

Department of Physics, Brookhaven National Laboratory,

Upton, New York, USA

Abstract

Recent results concerned with x-ray resonant magnetic scattering studies of the induced Lu magnetization in Dy-Lu alloys (Everitt et al., 1995) and of magnetic disordering of UO_2 surfaces (Watson et al., 1996) are reviewed.

1 Introduction

During the last 10 years, x-ray magnetic scattering techniques using synchrotron radiation have blossomed, especially in studies of rare earth metals and actinides, including bulk materials, thin films and compounds. These studies have especially benefited from the use of the resonance and polarization properties of the cross-section when the incident x-ray energy is tuned near an L or M absorption edge. Brief reviews of these techniques and recent applications may be found in Gibbs (1992) and Stirling and Lander (1992). Non-resonant magnetic scattering has also continued to develop, most notably in studies of transition element magnetism using incident photons of ≥ 40 keV (Schneider, 1995). In this case the enhancement to the signal comes from the increased penetration (up to cms) possible with high energy photons. Although the strengths of x-ray magnetic scattering techniques sometimes overlap those of neutron diffraction, they are generally complementary, and include high Q resolution, sensitivity to lattice modulations, small beam size and useful polarization and resonance properties. In the last 10 years x-ray magnetic scattering studies of the magnetic structure of rare earth and actinide materials (including thin films) have almost become routine (Hill et al., 1996; Detlefs et al., 1996; Helgesen et al., 1994, 1995). New kinds of experiments have been concerned with critical properties, characterized near magnetic ordering transformations (Nuttall et al., 1996; Thurston et al., 1994) and with the use of circularly polarized incident beams (Sutter et al., 1997).

In this proceedings, we briefly review recent experiments concerned with the induced Lu magnetization in Dy–Lu thin films (Everitt et al., 1995) and with the observation of surface magnetism in UO_2 (Watson et al., 1996; Ferrar et al., 1996).

2 Species sensitivity in Dy–Lu thin films

It is generally accepted that exchange interactions in the heavy rare-earth metals (Gd to Er) are indirect, arising through the agency of spin-density oscillations induced in the $5d$–$6s$ conduction bands by the localized $4f$ moments (Freeman, 1972). The conduction electron response peaks at a wave vector determined by nesting features in the Fermi surface and, in competition with the hexagonal crystal field, leads to the complex antiferromagnetic structures observed at low temperatures, including c-axis modulated, helical, cycloidal, and conical configurations (Cooper, 1972; Jensen and Mackintosh, 1991). Band structure calculations, indeed, give a good account of the periodicities observed near T_N (Evenson and Liu, 1969; Liu et al., 1971). However, direct evidence for the induced spin-density wave is sparse.

In early experimental work, Moon et al. (1972) were able to determine the conduction electron polarization in ferromagnetic Gd by subtracting from the observed neutron scattering intensity the component attributable to the half-filled $4f$ shell of Gd. Extra intensity was observed in low-order peaks which, when combined with the excess moment measured at saturation, yielded a map of the conduction electron polarization around each Gd ion and revealed its oscillatory nature. Similar methods have been used to map the magnetic response of non-magnetic Sc (Koehler and Moon, 1976) and Lu (Stassis et al., 1977) in a uniform field of order 6 T. In the case of Dy, which is of interest here, it is well known (Rhyne, 1972) that the saturation moment in the low-temperature ferromagnetic phase exceeds the 10 μ_B expected for the ${}^6H_{15/2}$ ground configuration by approximately 0.33 μ_B. The excess is usually attributed to the conduction electron polarization, and has been detected by means of x-ray resonant scattering (Hannon et al., 1988; Isaacs et al., 1989). However, the induced polarization of a non-magnetic atom has never been measured in the helimagnetic phase. These experiments demonstrate that it is possible to detect the conduction electron polarization induced on a non-magnetic atom in the helical phase of a rare-earth alloy by means of the resonant scattering of x-rays.

X-ray resonant magnetic scattering (XRES) (Hannon et al., 1988) is an element-specific technique that exploits the anomalous cross-section for x-ray scattering at an absorption edge. The XRES intensity is much larger, in general, than that of off-resonant scattering; the two processes also have different polarization characteristics. In the lanthanide series, the $L_{\rm III}$ edge lies in an energy range (7–10 keV)

that is convenient for diffraction studies. Near the edge energy, both dipole transitions from the $2p_{3/2}$ core level to unoccupied $5d$ states and quadrupole transitions to unoccupied $4f$ levels contribute significantly to the atomic form factor for x-ray scattering. Sensitivity to magnetic order arises from the differential occupancy of spin-up and spin-down states in the vicinity of the Fermi surface. Recently, studies of the binary magnetic-magnetic rare-earth alloys $Ho_{0.5}Er_{0.5}$ (Pengra et al., 1994) and $Ho_{0.5}Tb_{0.5}$ (Stunault et al., 1995) using this technique have been reported. For this work, the helimagnetic alloy $Dy_{0.6}Lu_{0.4}$ was chosen, which has been found via neutron scattering (Everitt et al., 1994) to order in a basal-plane spiral below 120 K. This alloy affords the opportunity to study the diffraction profiles at both the Dy (7.79 keV) and Lu (9.24 keV) $L_{\rm III}$ edges. Because Lu has a filled $4f$ shell, any scattered intensity that is resonant at the $L_{\rm III}$ edge must arise from magnetization of the $5d$ levels at the Lu site, and will therefore be a measure of the induced conduction electron polarization at the helimagnetic wave vector.

The elastic scattering cross-section for x-ray scattering from a single crystal is given by

$$\frac{d\sigma}{d\Omega} = r_0^2 \left| \sum_j e^{i\mathbf{Q}\cdot\mathbf{R}_j} \, f_j(\mathbf{Q},\omega) \right|^2 , \tag{1}$$

where r_0 is the classical radius of the electron; $\mathbf{Q} = \mathbf{k}_{\rm in} - \mathbf{k}_{\rm out}$, the photon momentum transfer; and $\hbar\omega$, the x-ray energy. The atomic scattering amplitude f_j consists of the usual Thomson contribution plus magnetic terms. The non-resonant magnetic amplitude may be written as

$$f_j^{\rm nonres} = \frac{i\hbar\omega}{2mc^2} [\mathbf{L}_j(\mathbf{Q}) \cdot \mathbf{A} + 2\mathbf{S}_j(\mathbf{Q}) \cdot \mathbf{B}] \, ; \tag{2}$$

the vectors $\mathbf{A}$ and $\mathbf{B}$ depend on the polarizations of the incoming and outgoing photons relative to their respective wave vectors. $\mathbf{L}_j(\mathbf{Q})$ and $\mathbf{S}_j(\mathbf{Q})$ are the Fourier components of the orbital and spin magnetization densities due to the jth atom (Blume, 1985; Blume and Gibbs, 1988). In a helimagnet, it has been shown (Gibbs et al., 1991) that the signal scattered from the σ to the π channel is due to the sum of orbital and spin densities.

The resonant scattering contributions are more complex (Hannon et al., 1988; Luo et al., 1993). The electric dipole contribution at the $L_{\rm III}$ edge has been treated in detail by Hannon et al. (1988) and can be approximated by

$$f_j^{E1,{\rm xres}} = \frac{F_0}{E_{L_{\rm III}} - \hbar\omega - i\Gamma/2} \left[\hat{\mathbf{e}}_{\rm out} \cdot \hat{\mathbf{e}}_{\rm in} \, n_h + i(\hat{\mathbf{e}}_{\rm out} \times \hat{\mathbf{e}}_{\rm in}) \cdot \hat{\mathbf{z}}_j P/4 \right] . \tag{3}$$

Here, F_0 includes the $2p_{3/2} \rightarrow 5d$ radial matrix element, $E_{L_{\rm III}}$ is the edge energy, and Γ is the width of the resonance. The magnetic moment of the jth ion is parallel

to $\hat{\mathbf{z}}_j$. The first term, which depends on the number n_h of holes of both spins, does not reflect the magnetic order. The polarization factor can be written as

$$P = (n_{d\uparrow} - n_{d\downarrow}) - n_h\delta - \frac{n_h\Delta/2}{E_{L_{\rm III}} - \hbar\omega - i\Gamma/2}\,, \tag{4}$$

where $n_{d\uparrow} - n_{d\downarrow}$ is the net number of magnetized $5d$ electrons, δ depends on the difference in radial matrix elements for spin-up and spin-down electrons, and Δ is the exchange splitting. At this level of approximation, the magnetic reflections appear only as first-order satellites of the main Bragg peaks, and only in the $\sigma \rightarrow \pi$ channel.

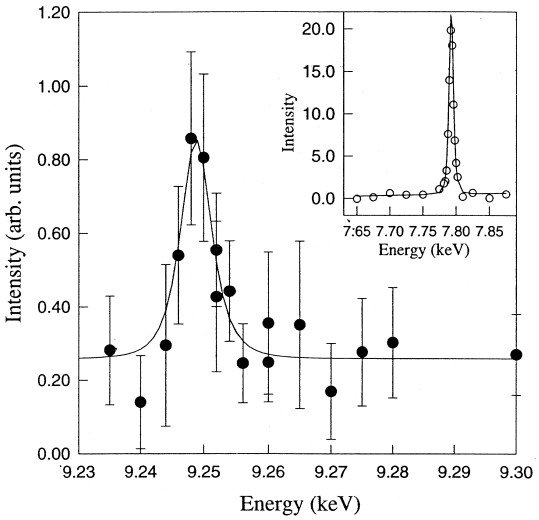

Figure 1. Q-integrated intensity of the (0002+τ) magnetic peak vs energy through the Lu $L_{\rm III}$ edge. Residual intensity is attributed to the non-resonant scattering from the Dy moments. Inset: The same, measured through the Dy $L_{\rm III}$ edge. An MgO(420) analyzer was used for both measurements. Lorentzian-squared curves with a FWHM of 7 eV have been fit to both data sets.

X-ray resonant magnetic scattering was observed at both the Dy and Lu edges in the $\sigma \rightarrow \pi$ geometry, consistent with dipole selection rules. The same crystal was used at both energies in order to compare directly the magnitudes of the resonant intensities. First-order helimagnetic satellites were detected about the (0002), (0004), and (0006) Bragg reflections of the alloy; they are designated as (000$\ell\pm\tau$).

At low temperatures, these were separated from the Bragg peaks by $\tau \simeq 0.24$ reciprocal lattice unit (rlu), in agreement with earlier neutron scattering data from the same sample (Everitt et al., 1994). We focus mainly on the $(0002+\tau)$ magnetic reflection, since the resonant scattering is more intense than at the $(0004\pm\tau)$ or $(0006\pm\tau)$ reflections and the background is lower than at the $(0002-\tau)$ reflection. Figure 1 shows the Q-integrated intensity of the $(0002+\tau)$ peak at 10 K as the energy was scanned through the Lu $L_{\rm III}$ edge (main figure) and the Dy $L_{\rm III}$ edge (inset). The data are normalized to monitor counts, with the energy dependence of the monitor efficiency taken into account, and are corrected for the Lorentz factor. Polarization and Debye–Waller corrections, which amount to $\cong 1\%$ of the intensity each, were not applied. Absorption was also not taken into account. The presence of resonant magnetic scattering at the Lu edge demonstrates the existence of an induced moment on the Lu atoms. The $\sigma \rightarrow \pi$ character of the scattering shows that it occurs within the Lu $5d$ band. Estimates of the induced Lu moment obtained using Eqs. (3) and (4) give an SDW amplitude of $\sim 0.2\ \mu_B$.

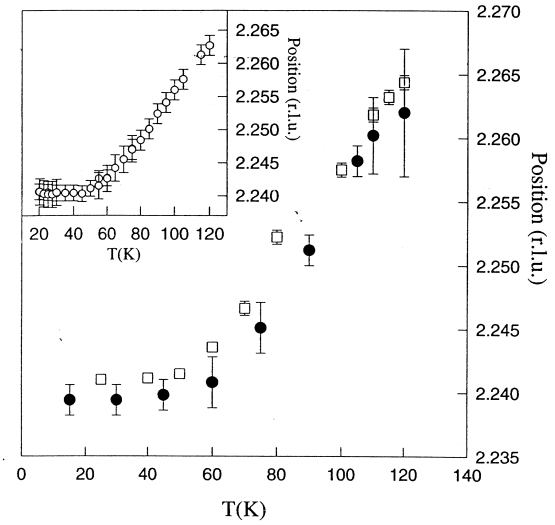

Figure 2. Magnetic wave vector τ in units of the c-axis reciprocal lattice vector, determined from the $(0002+\tau)$ peak. Solid circles: XRES data at the Lu edge in the $\sigma \rightarrow \pi$ configuration; squares: previous neutron scattering data. Inset: XRES data at the Dy edge, measured in the scattering plane, using a Ge analyzer for higher resolution. Below 60 K, a lock-in occurs to a value near 0.240 rlu.

Figure 2 shows the position of the (0002+τ) magnetic peak (filled circles) as a function of temperature, with the neutron scattering data of Everitt et al. (1994) superposed. The helimagnetic wave vector is $\cong 0.265$ **c*** at the Néel temperature $T_N = 120$ K, and decreases with temperature before appearing to lock in to 0.240 ± 0.001 **c*** ($\cong 6/25$) below $\simeq 60$ K. This may be seen more clearly in the inset to Fig. 2, where the position of the same reflection, measured at the Dy edge using a Ge(111) analyzer for better resolution, is plotted. This is a considerably tighter spiral than observed (Koehler, 1972) in bulk Dy, where the wave vector is 0.239 **c*** at T_N decreasing to 0.147 **c*** at the Curie temperature $T_C = 89$ K.

The temperature dependence of the (0002+τ) magnetic peak is shown in Fig. 3. In this figure, the Dy data were taken in the high-resolution mode (Ge analyzer) and the Lu data in the $\sigma \rightarrow \pi$ mode (MgO analyzer). Neutron scattering data are shown in the inset, for reference. Lines are drawn as a guide to the eye. These results show that the temperature dependence of the $5d$ magnetization density induced at the Lu and Dy sites follows that of the Dy $4f$ moments in the alloy.

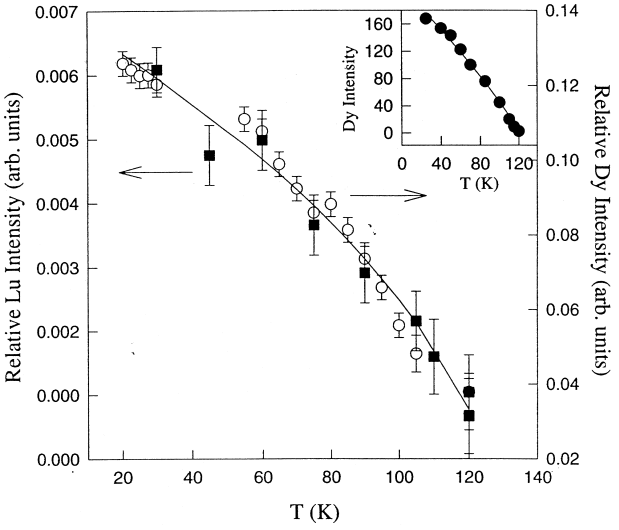

Figure 3. Temperature dependence of the (0002+τ) magnetic peak. Squares: Lu-edge data taken in the $\sigma \rightarrow \pi$ geometry; circles: Dy-edge data, taken in high resolution mode. Inset: Neutron diffraction data for the same sample.

3 UO_2 surfaces

In the last several years, there have been continuing efforts to probe long ranged magnetic order at surfaces by x-ray and neutron diffraction (Felcher et al., 1984; Usta et al., 1991; Kao et al., 1990; Fasolino et al., 1993; Bernhoeft et al., 1996; Stunault et al., unpublished; Watson et al., 1996), following many earlier studies by low energy electron diffraction (Palmberg et al., 1968; Dewames and Wolfram, 1969; Celotta et al., 1979; Alvarado et al., 1982; Dauth et al., 1987). The main motivation has been to discover how bulk magnetic structures are modified near a surface, where the crystal symmetry is broken. In this section, we describe synchrotron-based x-ray scattering studies of magnetic ordering near the (001) surface of the type-I antiferromagnet UO_2. Our aim in choosing UO_2 was twofold: first, to take advantage of its chemical inertness, which simplifies the preparation and handling of the surface; and second, to take advantage of the large resonant enhancements of the magnetic cross-section which occur when the incident photon energy is tuned near the uranium $M_{\rm IV}$ absorption edge (McWahn et al., 1990). We have found that it is possible to observe x-ray magnetic scattering from UO_2 surfaces at glancing incident angles (Watson et al., 1996) near the critical angle for total external reflection, with counting rates as high as 200 s^{-1} on a wiggler beam line. This has allowed characterization of the momentum transfer dependence of several magnetic (and charge) truncation rods along the surface normal. By tuning the incident x-ray energy through the $M_{\rm IV}$ edge, we have verified that the observed scattering is magnetic, and extracted forms for the variation of f' and f'' with x-ray energy. A most interesting result is that within about 50 Å of the surface, the temperature dependence of the magnetic scattering intensity decreases continuously near the Néel temperature $T_N = 30.2$ K and is well described by a power law in reduced temperature. In contrast, the bulk magnetic order parameter is well known to be discontinuous (Frazer et al., 1965; Willis and Taylor, 1965).

UO_2 has the face-centered cubic fluorite structure with a lattice constant of 5.47 Å at 300 K. The allowed chemical Bragg reflections are defined by H, K, and L either all even or all odd. The diffraction pattern of a crystal supporting a surface is characterized by rods of scattering (called truncation rods) which pass through the allowed bulk Bragg points and are parallel to the surface normal (see Fig. 4(a)). The variation of the x-ray intensity along the chemical truncation rods is determined by the decay of the electronic charge density near the surface (Feidenhans'l, 1989). The bulk magnetic structure of UO_2 is triple $\mathbf{Q}$, consisting of ferromagnetic (001)-type planes stacked antiferromagnetically along each of the $\langle 001 \rangle$ directions. The magnetic bulk reflections are obtained by adding a $\langle 001 \rangle$ wave vector to each allowed chemical Bragg wave vector (see Fig. 4(a)). We may similarly define magnetic truncation rods (Fasolino et al., 1993), which pass through

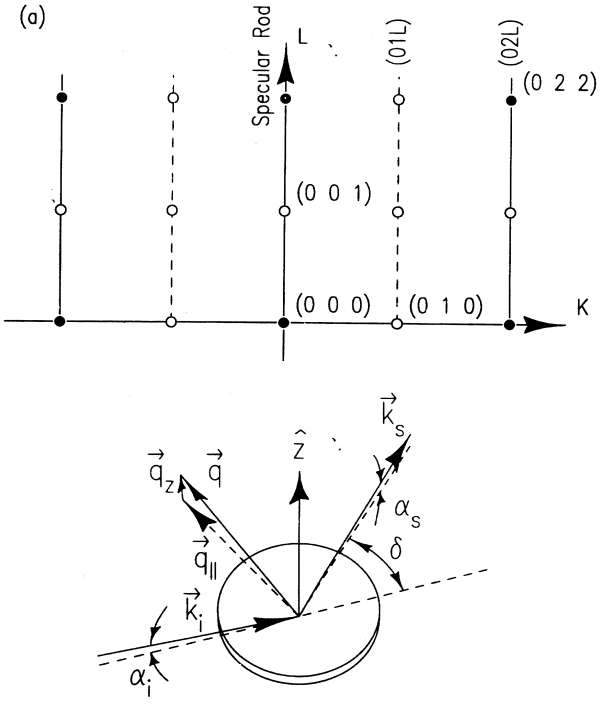

Figure 4. (a) Reciprocal space map for the UO_2 (001) surface showing chemical (solid circles) and magnetic (open circles) bulk Bragg reflections and mixed (solid lines) and magnetic (dashed lines) truncation rods. (b) Glancing-incidence scattering geometry. $\hat{z}$ is the surface normal direction, $\vec{k}_i$, $\vec{k}_s$, and $\vec{q}$ are the incident, scattered, and transferred wave vectors, respectively. $\vec{q}_z$ is the component of the momentum transfer normal to the surface.

the bulk magnetic reflections, and whose intensity variation depends on the decay of the magnetization density near the surface. For an antiferromagnet, this leads both to magnetic contributions to the chemical rods as well as to the existence of pure magnetic truncation rods when H and K are mixed (see Fig. 4(a)). The primary aim of the present experiments was to observe the $(01L)$ magnetic rod.

The scattering geometry is illustrated in Fig. 4(b). Most of the experiments were carried out at glancing incidence, where the incident and exit angles of the x-ray beam to the surface are near the critical angle $\alpha_c \sim 0.75°$ for total external reflection. Near α_c, the refraction effects become important and lead to an enhancement of the transmitted beam. These effects are well understood (Feidenhans'l, 1989) and illustrated in the top of Fig. 5(a) where the intensity dependence

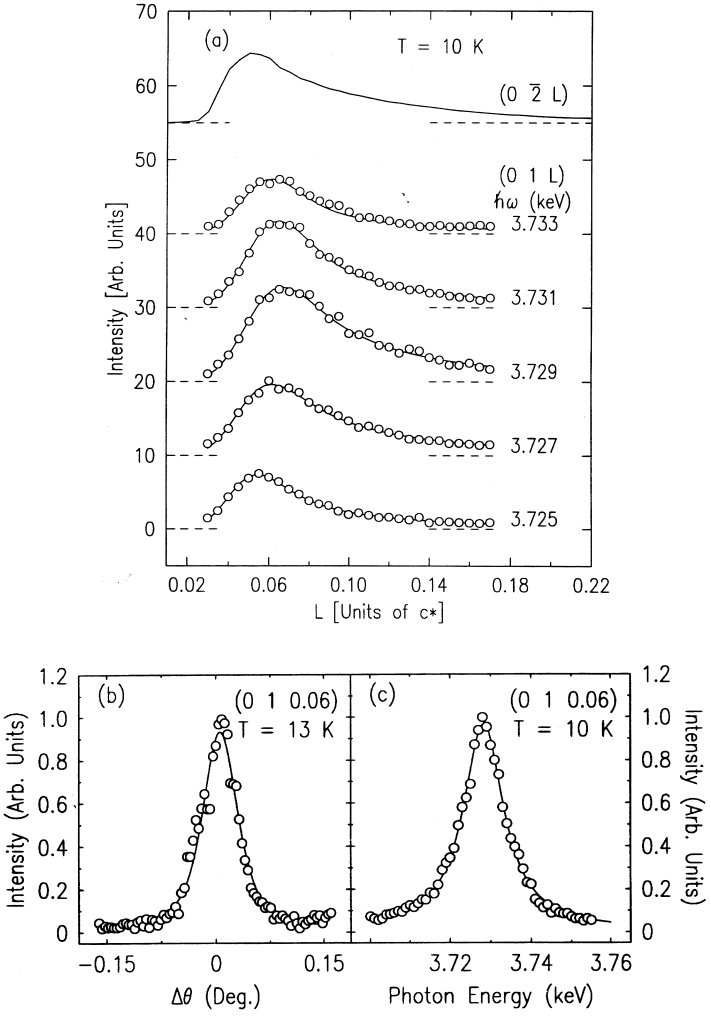

Figure 5. Intensity of the $(0\bar{2}L)$ charge (solid line, and $(01L)$ magnetic (open points) truncation rods as a function of L. The magnetic rod was obtained at five photon energies. The $(0\bar{2}L)$ rod was obtained with an incident photon energy of 3.728 keV. (b) Rocking curve of the magnetic truncation rod at $L = 0.06$. (c) Energy dependence of the intensity of the magnetic truncation rod at $L = 0.06$.

of the $(0\bar{2}L)$ charge scattering rod is shown. The intensity along the rod may be described by

$$I(k_i, k_s)/I_0 = (I/A_0) \mid T(\alpha_i) \mid^2 \mid T(\alpha_s) \mid^2 \left(\frac{d\sigma}{d\Omega}\right), \tag{5}$$

where A_0 and I_0 are the area and flux of the incident beam and $T(\alpha)$ is the usual Fresnel transmission amplitude for x rays at an angle α to the surface. $d\sigma/d\Omega$ is the cross-section for x-ray scattering and depends on the Fourier transform of the electronic charge density. Near the critical angle, the transmission coefficients exhibit maxima which lead to the peak observed in Fig. 5(a).

The lower curves in Fig. 5(a) show the intensity dependence of the pure magnetic scattering along the $(01L)$ rod, obtained as a function of incident photon energy. Their shapes are all qualitatively similar to that of the charge scattering. Rocking curves taken through the magnetic rod at $L = 0.06$ (see Fig. 5(b)) give full widths of 0.06°, identical to that of the charge scattering rod, and close to the bulk mosaic. No variation in rocking width was observed along the rods. All of this indicates that the in-plane magnetic structure near the surface is well ordered at 10 K. The energy dependence of the magnetic intensity at fixed L is summarized in Fig. 5(c). The observed resonance is identical to that obtained in other uranium compounds and shows that the observed scattering is magnetic in origin.

We turn now to the temperature dependence of the magnetic scattering. Figure 6 shows the intensity plotted versus temperature as obtained at two positions along the magnetic truncation rod, (0,1,0.075) and (0,1,0.15), and at the bulk (001) reflection. From the measured dispersion corrections to the atomic form factors, it may be shown that these values of (HKL) correspond to penetration depths of ~ 50, ~ 120, and ~ 850 Å, respectively. The temperature dependence of the magnetic scattering at the (001) reflection exhibits the discontinuity at T_N expected from previous studies (Frazer et al., 1965; Willis and Taylor, 1965). In contrast, the magnetic scattering intensities obtained on the truncation rod fall more slowly to zero as T_N is approached from below. Indeed, they appear continuous. It is worth noting that the width of the magnetic truncation rods are temperature independent and, to within ±0.5 K, the bulk and near surface ordering temperatures are equal. These results suggest that the magnetic structure *begins* to disorder at lower temperatures near the surface than in the bulk. This conclusion is similar to that obtained by Dosch and co-workers in their x-ray structural studies of the order-disorder transition in Cu_3Au (Dosch et al., 1988; Dosch and Peisl, 1989; Dosch et al., 1991; Reichert et al., 1995). In those experiments, the near-surface superlattice peak of the ordered alloy was found to decay continuously near T_0 (the order-disorder temperature), whereas the bulk behaviour was discontinuous. They interpreted their results in terms of surface-induced disordering, wherein a

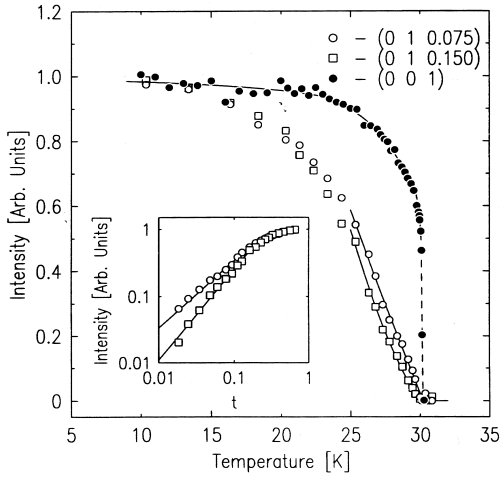

Figure 6. Magnetic intensities obtained at the (001) specular Bragg reflection (solid circles) and along the (01L) magnetic truncation rod at $L = 0.075$ (open circles) and 0.15 (open squares). They have been normalized to 1.0 at low temperatures. The solid lines represent best fits to a power law dependence on reduced temperature. The solid line for the (001) reflection is a guide for the eye. Inset: log–log plot of the magnetic scattering intensity at (0,1,0.075) and (0,1,0.15) vs reduced temperature.

partially disordered layer of crystalline phase wets the near-surface volume below T_0 and grows logarithmically in thickness as T approaches T_0. Surface-induced disorder was introduced for first-order transitions by Lipowsky (Lipowsky, 1982; Lipowsky and Speth, 1983) and has been discussed in many contexts since (Dietrich, 1988; Mecke and Dietrich, 1995, and references therein). Within Landau theory, these calculations yield regions of the phase diagram for which the order parameter at the surface is predicted to follow a power law in reduced temperature.

Motivated by these ideas, we have attempted a similar analysis in UO_2. Fits of the magnetic scattering intensity to a power law in reduced temperature, $I = At^{2S}$, where $t = (T_N - T)/T_N$, are shown for two values of L by the solid lines in Fig. 6. The fits are clearly satisfactory and yield exponents $S = 0.5 \pm 0.1$ at $L = 0.075$ and $S = 0.7 \pm 0.15$ at $L = 0.150$. Evidently, the exponents exhibit an L dependence, *increasing* for increasing δL (δL referred to the nearest Bragg peak), which differs from trends observed in Cu_3Au and from the predictions of Lipowsky's theory. More sophisticated models, for example, including a temperature-dependent width to the interface between the ordered and disordered magnetic regions (Lipowsky, 1987), have not resolved this distinction. In this regard, it is important to note

that the intensity measured along a truncation rod depends on the order parameter profile along the surface normal and reduces to the square of the average order parameter only when the atomic planes scatter in phase. Thus while our results are qualitatively consistent with the ideas of surface-induced disordering, a quantitative description of UO_2 remains lacking.

4 Conclusions

This proceedings has briefly reviewed two recent developments in x-ray scattering studies of magnetic materials. Ongoing efforts continue both in thin films and on surfaces, as well as in other areas not mentioned here for lack of space. The long term prospects for these techniques seem very exciting indeed.

5 Acknowledgements

With a mixture of pleasure and sadness, the author acknowledges many helpful discussions over the years with Allan Mackintosh; we will miss him. The author also gratefully acknowledges his collaborators in the work reviewed in this article, especially B. Everitt, M. Salamon, B.J. Parks, C.P. Flynn and T.R. Thurston (Everitt et al., 1995); and G.M. Watson, G.H. Lander, B. Gaulin, L. Berman, H. Matzke, and W. Ellis (Watson et al., 1996). Work performed at Brookhaven is supported by the U.S. Department of Energy under contract No. DE-AC02-76CH00016.

References

Al Usta K et al., 1991: Physica B **173B**, 65
Alvarado SF, 1982: Phys. Rev. Lett. **48**, 51
Bernhoeft N et al., 1995: J. Magn. Magn. Mater. **140**, 1421
Blume M, 1985: J. Appl. Phys. **57**, 3615
Blume M and Gibbs Doon, 1988: Phys. Rev. B **37**, 1779
Celotta RJ, 1979: Phys. Rev. Lett. **43**, 728
Cooper BR, 1972: *Magnetic Properties of Rare-Earth Metals*, ed. R.J. Elliott (Plenum Press, London) Chap. 2
Dauth B et al., 1987: Surf. Sci. **189/190**, 729
Detlefs C et al., 1996: Phys. Rev. B **53**, 6355
Dewames RE and Wolfram T, 1969: Phys. Rev. Lett. **22**, 137
Dietrich S, 1988: *Phase Transitions and Critical Phenomena*, eds. C. Domb and J.L. Lebowitz (Academic, New York) **12**
Dosch H et al., 1988: Phys. Rev. Lett. **60**, 2382
Dosch H and Peisl J, 1989: Colloq. Phys. **50**, C7-257
Dosch H et al., 1991: Phys. Rev. B **43**, 13172

Evenson WE and Liu SH, 1969: Phys. Rev. **178**, 783
Everitt B et al., 1995: Phys. Rev. Lett. **75**, 3182
Everitt BA, Salamon MB, Flynn CP, Park BJ, Borchers JA, Erwin RW and Tsui F, 1994: J. Appl. Phys. **75**, 6592
Fasolino A et al., 1993: Phys. Rev. B **47**, 3877
Feidenhans'l R, 1989: Surf. Sci. Rep. **10**, 105
Felcher GP et al., 1984: Phys. Rev. Lett. **52**, 1539
Ferrar S et al., 1996: Phys. Rev. Lett. **77**, 747
Frazer BC et al., 1965: Phys. Rev. **140**, 1448
Freeman AJ, 1972: *Magnetic Properties of Rare-Earth Metals*, ed. R.J. Elliott (Plenum Press, London) Chap. 6
Gibbs D, 1992: Synchrotron Radiation News **5**, 18
Gibbs D et al., 1991: Phys. Rev. B **43**, 5663
Hannon JP, Trammel GT, Blume M and Gibbs D, 1988: Phys. Rev. Lett. **61**, 1245
Helgesen G, Hill JP, Thurston TR, Gibbs D, Kwo J and Hong M, 1994: Phys. Rev. B **50**, 2990
Helgesen G et al., 1996: Phys. Rev. B **52**, 9446
Hill JP, Sternlieb B, Gibbs D, Detlefs C, Goldman A, Stassis C, Canfield P and Cho B, 1996: Phys. Rev. B **53**, 3487
Isaacs ED, McWhan DB, Siddons DP, Hastings JB and Gibbs D, 1989: Phys. Rev. B **40**, 9336
Jensen J and Mackintosh AR, 1991: *Rare Earth Magnetism: Structures and Excitations* (Clarendon Press, Oxford)
Kao CC et al., 1990: Phys. Rev. Lett. **65**, 373
Koehler WC, 1972: *Magnetic Properties of Rare-Earth Metals*, ed. R.J. Elliott (Plenum Press, London) p. 81
Koehler WC and Moon RM, 1976: Phys. Rev. Lett. **36**, 616
Lipowsky R, 1987: Ferroelectrics **73**, 69
Lipowsky R, 1982: Phys. Rev. Lett. **49**, 1575
Lipowsky R and Speth W, 1983: Phys. Rev. B **28**, 3983
Liu SH, Gupta RP and Sinha SK, 1971: Phys. Rev. B **4**, 1100
Luo Jin, Trammell GT and Hannon JP, 1993: Phys. Rev. Lett. **71**, 287
McWahn DB et al., 1990 Phys. Rev. B **42**, 6007
Mecke KR and Dietrich S, 1995: Phys. Rev. B **52**, 2107
Moon RM, Koehler WC, Cable JW and Child HR, 1972: Phys. Rev. B **5**, 997
Nuttall WJ, Langridge S, Stirling WG, Lander GH, Lebech B and Vogt O, 1996: Phys. Rev. B (in press)
Palmberg PW et al., 1968: Phys. Rev. Lett. **21**, 682
Pengra DB, Thoft NB, Wulff M, Feidenhans'l R and Bohr J, 1994: J. Phys. Condens. Matter **6**, 2409
Reichert H et al., 1995: Phys. Rev. Lett. **74**, 2006
Rhyne JJ, 1972: *Magnetic Properties of Rare-Earth Metals*, ed. R.J. Elliott (Plenum Press, London) p. 131.
Schneider J, 1995: Synchrotron Radiation News **8**, No. 2, 26
Stassis C, Kline BR, Loong CK and Harmon BN, 1977: Solid State Commun. **23**, 159
Stirling WG, and Lander GH, 1992: Synchrotron Radiation News **5**, 17
Stunault A, Vettier C, de Bergevin F, Maier F, Grübel G, Galéra RM and Palmer SB, 1995: J. Magn. Magn. Mater. **140-144**, 753
Stunault A, Langridge S, Vettier C, Gibbs D and Bernhoeft N, 1996: Phys. Rev. B (in press)
Sutter C, Grübel G, Vettier C, de Bergerin F, Stunault A, Gibbs D and Giles C, 1997: Phys. Rev. B (in press)
Thurston T, Helgesen G, Hill JP, Gibbs D, Gaulin BD and Simpson P, 1994: Phys. Rev. B **49**,

15730
Watson GM et al., 1996: Phys. Rev. Lett. **77**, 751
Watson GM et al., 1996: Physica B **221**, 405
Willis BTM and Taylor RI, 1965: Phys. Lett. **17**, 188